Meta Gene 2 (2014) 557–564

Contents lists available at ScienceDirect

Meta Gene

SLC34A2 gene compound heterozygous mutation identification in a patient with pulmonary alveolar microlithiasis and computational 3D protein structure prediction

Huiying Wang [a,*], Xinzhen Yin [a], Dingwen Wu [b], Xinguo Jiang [c]

[a] *Department of Allergy and Clinical Immunology, the Second Affiliated Hospital, College of Medicine, Zhejiang University, Hangzhou 310009, China*
[b] *The Children's Hospital, College of Medicine, Zhejiang University, Hangzhou, China*
[c] *Department of Medicine, VA Palo Alto Health Care System, Stanford University School of Medicine, Stanford, CA, 94305, USA*

ARTICLE INFO

Article history:
Received 12 April 2014
Revised 22 July 2014
Accepted 24 July 2014
Available online 15 August 2014

Keywords:
SLC34A2
Autosomal recessive
Computational prediction
Protein structure

ABSTRACT

We recently diagnosed a patient with pulmonary alveolar microlithiasis (PAM). Because loss-of-function mutations of the *SLC34A2* gene are responsible for the development of PAM, we sought to sequence the *SLC34A2* gene of the patient and his direct relatives, with a purpose to identify mutations that caused the PAM of the patient as well as the carriers of his family. We found a novel compound heterozygous mutation of the *SLC34A2* gene in this patient, which were the mutations of c.1363T > C (p. Y455H) in exon 12 and c.910A > T (p. K304X) in exon 8. Computational prediction of three-dimensional (3D) structures of the mutants revealed that the Y455H mutation resulted in a formation of irregular coils in the trans-membrane domain and the K304X mutation resulted in protein truncation. Our study suggested that sequencing of the *SLC34A2* gene together with a computational prediction of the 3D structures of the mutated proteins may be useful in PAM diagnosis and prognosis.

Introduction

Pulmonary alveolar microlithiasis (OMIM [Online Mendelian Inheritance in Man] 265100) is a rare disease characterized by diffuse alveolar deposition of microliths (Ucan et al., 1993). PAM was first described by Malpighi in 1686 and named by Puhr in 1933 (Puhr, 1933). Since then, more than 500 cases

* Corresponding author. Tel.: +86 571 87783267; fax: +86 571 87783516.
E-mail address: w_huiying@yahoo.com (H. Wang).

http://dx.doi.org/10.1016/j.mgene.2014.07.004

have been reported all over the world (Mariotta et al., 2004). Among these patients, about one-third of them are familial. One remarkable feature of PAM is the late onset of symptoms despite the fact that it causes diffuse lung lesions. This is probably also the main reason why PAM is often incidental to other clinical diagnosis (Mariotta et al., 2004).

SLC34A2 is a type IIb sodium phosphate co-transporter which primarily expresses in alveolar type II cells. It is also the only known sodium-dependent phosphate transporter expressed in the lung. This protein plays a key role in clearing phospholipids of the alveolar space through transporting the phosphorus ion into the alveolar type II cells (Hashimoto et al., 2000). Mutations that cause SLC34A2 dysfunction or deficiency could therefore result in an accumulation of the local phosphate in lung parenchyma, which may represent the main mechanism associated with the microlith formation. In 2006, Corut et al. first identified a PAM locus on chromosome 4p15 by homozygosity mapping, and proposed that the mutation of the *SLC34A2* gene causes PAM (Corut et al., 2006). Huqun et al. employed a modified homozygosity mapping method and discovered homozygous exonic mutations on exon 8 of the *SLC34A2* gene in PAM patients they examined (Huqun et al., 2007). Other studies from Turkey, Japan and China have also described multiple mutations of this gene in PAM patients (Dogan et al., 2010; Ishihara et al., 2009; Ozbudak et al., 2012; Proesmans et al., 2012; Tachibana et al., 2009; Wang et al., 2010). However, the functions of these mutated proteins were not analyzed because of the poor understanding of their structures. Here we not only identified the mutations that caused PAM in this patient, but also computationally predicted 3D structures of these mutants. Our study may provide a novel strategy to help diagnose patients who may potentially develop PAM; it may also be used to estimate the prognosis.

Methods

Case report

A 43-year-old man from a non-inbred family was admitted to the hospital complaining of recurrent dyspnea for 1 year. The symptom started as mild chest tightness but deteriorated significantly within a year. He was healthy in the past and denied any history of medication. He had a history of smoking for 20 years with 20 cigarettes per day. His parents are not consanguineous, and he has a sister and a son. None of them complained of discomfort and their chest CT scans were normal.

Physical examination upon admission revealed apparent cyanosis of lips, venous varicose and slight bulb fingers. Crackle rales were heard in both lung fields. Laboratory tests revealed an increased level of hemoglobin (171 g/L) and a decreased level of PaO_2 (49.3 mm Hg); the serum calcium concentration and the tumor index panel were within the normal range. Ultrasound cardiogram showed enlargement of the right ventricle with severe pulmonary arterial hypertension. The dilation function of the left ventricle was found declined. Spirometry exam showed severe restrictive ventilatory disturbances and a decreased diffusing capacity (vital capacity, 44.2% of predicted, forced expiratory volume in 1 s, 84.4% of predicted, carbon monoxide transfer factor-single breath, 42.0% of predicted). Bronchoalveolar lavage fluid (BALF) was milky with negative Rivalta test. Smear of BALF showed fine sand inside. Chest computed tomography (CT) scan showed a diffused infiltration of fine sand-stones in both lungs mainly in the upper fields, and with interstitial changes in lower lung fields (Fig. 1A–D). Trans-bronchial lung biopsy showed lamellar microliths deposited in alveolar spaces and the pleura (Fig. 2A, B). The diagnosis of PAM was therefore established based on the symptoms, thorax imaging and the biopsy.

Genetic analysis

Genomic DNA was extracted from peripheral blood of the patient and his relatives as we previously described (Yin et al., 2013). The study was approved by the Ethics Committee of the second affiliated hospital, Zhejiang University School of Medicine (Ethic No. 2011-7), with a written consent form obtained from the subjects. Using the online software Primer3, 12 pairs of primers (Table 1) were designed to amplify the coding exons and the intronic flanking sequences of the *SLC34A2* gene. The amplifications were performed in thermocyclers (PerkinElmer, Inc, Foster City, CA, USA), starting with an

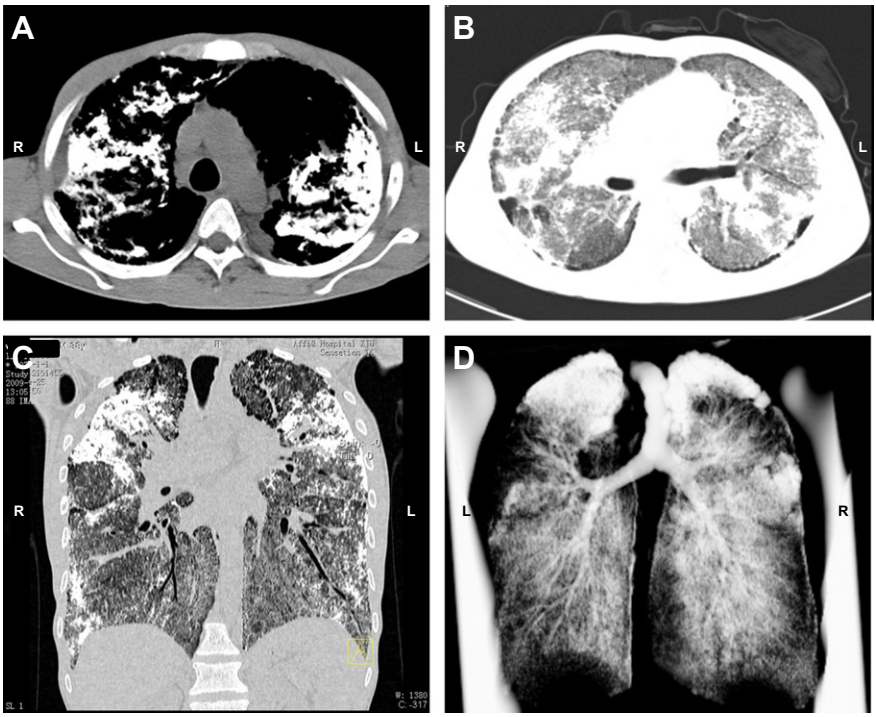

Fig. 1. High-resolution computed tomography (CT) of chest. Axial CT image shows extensive micronodular opacity within the lung parenchyma; signs of fibrosis and interstitial thickening were also seen. (A) Upper lung, mediastinal window. (B) Lower lung, lung window. (C) Coronal multiplanar reformation images. (D) Transparency view of the lungs shows diffuse symmetric involvement of both lungs, with a predominant distribution of micromodular opacity in the upper lobes.

initial denaturation of 4 min at 95 °C followed by 12 cycles of 35 second denaturation and 35 second annealing at 60 °C (0.5 °C decrease in each cycle), and 40 second extension at 72 °C. DNA sequencing was then performed in an ABI 3100 Genetic analyzer (Applied Biosystems, Invitrogen, Shanghai). All identified disease-associated variants were examined for their presence in controls (100 healthy volunteers/200 chromosomes).

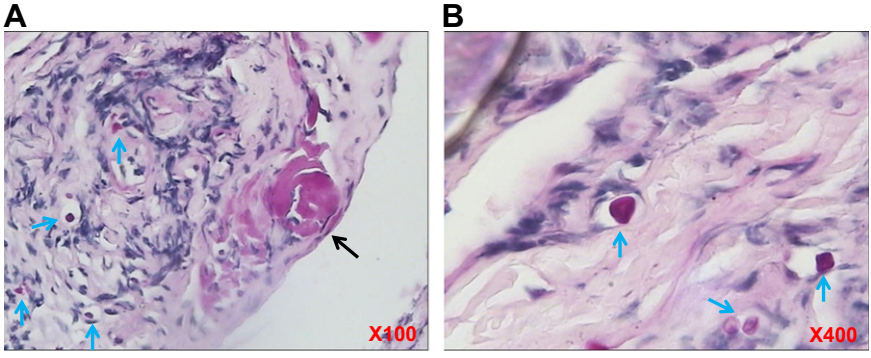

Fig. 2. H & E staining of transbronchial biopsy specimens. Deposition of concentrically laminated, partially calcified spheroid bodies in the visceral pleura (A) and alveolar space (A, B). (Black arrow, pleural microliths; blue arrows, alveolar microliths; magnifications, A, ×100; B, ×400).

Table 1
Sequences of primers and length of the amplicons.

Sequences of primers	Length of the amplicons
SLC34A2-1F: CCGTCGGAGCTTTTCTCTCGG	477 bp
SLC34A2-1R: GTCGATCGTAAGAGTGTAGCAGC	
SLC34A2-2-3F: GTTGATGCTTTGCAACCAATGG	500 bp
SLC34A2-2-3R: TGATGACACCCACAGTGAACG	
SLC34A2-4F: GCTCATTGCCAAACTTCTCAGG	300 bp
SLC34A2-4R: GCTGGAGAGGGCTTGCTGA	
SLC34A2-5F: GGCCTTGGATGGAGACTTCTG	302 bp
SLC34A2-5R: TCCCACCCTCAGATAGACAGG	
SLC34A2-6F: GGTAACTTTAGCCTGCCTCCAG	270 bp
SLC34A2-6R: GCATGTCATCTTTGGCTGGTT	
SLC34A2-7F: GAGGGTGGCAGATGATACAGG	357 bp
SLC34A2-7R: TGTCAGCTCAGGTAGGGGATG	
SLC34A2-8F: CCCTGGGTTTGTGTCCTAAATC	243 bp
SLC34A2-8R: CTTCCTTGAAGGCAAGATTTAGTT	
SLC34A2-9F: CATTGCCTCCCATTCCCCACT	241 bp
SLC34A2-9R: AATAGGTCACCCCCAGACAAC	
SLC34A2-10F: TAACAATCTGTAGCCGTGGTGG	300 bp
SLC34A2-10R: GAATCTAAAGGACCCCCACAC	
SLC34A2-11-12F: TGTACAACCTCACCCCTAAGCC	499 bp
SLC34A2-11-12R: AGAGACCAGTTTGCAAGACCATG	
SLC34A2-13-1F: TGTGATGCCTGCTAGCTTACCT	492 bp
SLC34A2-13-1R: CAGCAGCGCATCTGGAAGCAG	
SLC34A2-13-2F: CTGCCGAAGAAACTCCAGAACT	481 bp
SLC34A2-13-2R: CCAAAGGGAATCGAGTTAGGTAG	

Computational prediction of 3D structures of the mutated proteins

The functional impairment of the mutated proteins was evaluated computationally using web-based software programs. The bioinformation includes the hydrophobicity and the trans-membrane topological structure. ProtScale (*http://ca.expasy.org/tools/protscale.html*) was used to analyze the hydrophobicity; SOPMA from Centre National de la Recherche Scientifique (CNRS) was used to evaluate the secondary structure; and SMART (*http://smart.embl-heidelberg.de*) was used to assess the trans-membrane domains. The 3D structures of the wild-type SLC34A2 and the mutants were predicted by protein folding recognition with 3D-pssm (Phyre Version0.2). The initial 3D structures were acquired *via modeler 9.11,* and the structure optimization and the dynamic simulation were done via the software *Material Studio* (minimizer and dynamics program) (Kelley et al., 2000; Sali and Blundell, 1993). Procheck was used to verify the quality of the predicted protein structures (Vaguine et al., 1999).

Results

Identification of a compound heterozygous mutation

A compound heterozygous mutation was identified in the patient. One is c.1363T > C (p. Y455H) in exon 12, which is also seen in his mother, son and sister (a, b, d and e of Fig. 3A). The other is c.910A > T (p.K304X) in exon 8, which was also seen in his father (a and c of Fig. 3B). Analysis of 100 healthy volunteers did not show these mutations (f of Fig. 3A and B). Based on these findings, we created a pedigree for this family (Fig. 3C). It is clear that this patient carries a compound heterozygous mutation.

Computational prediction of 3D structures of the mutated proteins

Because functional examination of mutated proteins in a biological system is time-consuming and expensive, and the crystal structure of the SLC34A2 protein has not been solved, we reasoned that computational 3D structure prediction may provide useful information about the SLC34A2 protein and its mutants, which may also help assess the function of mutated proteins in a quicker and more efficient way.

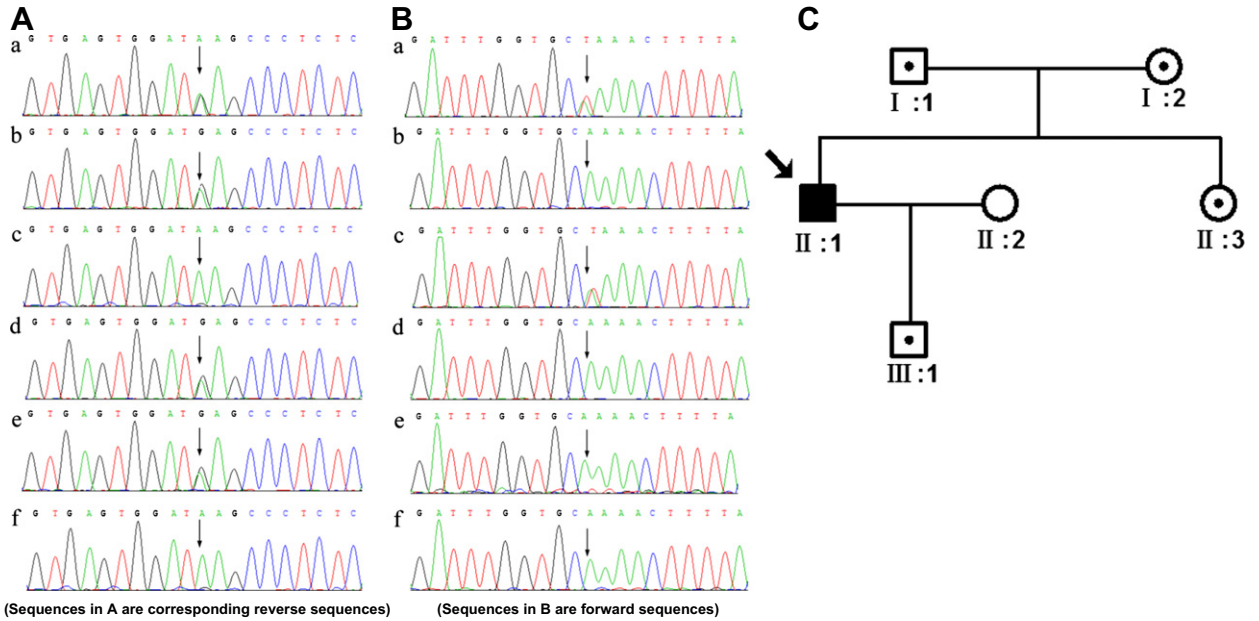

Fig. 3. Genetic analysis and the pedigree structure of the family with PAM. (A) The mutation of c.1363T > C (p. 455Y > H) in exon 12 (sequences shown in this panel are corresponding reverse sequences). (B) The mutation of c.910A > T (p. K304X) in exon 8. (a, The PAM patient; b, the mother of the patient; c, the father of the patient; d, the son of the patient; e, the sister of the patient; f, normal control). (C) Pedigree structure of the family. (Square symbols, men; circular symbols, women; filled symbols, PAM affected; dotted symbols, mutant carrier. The proband is marked by an arrow).

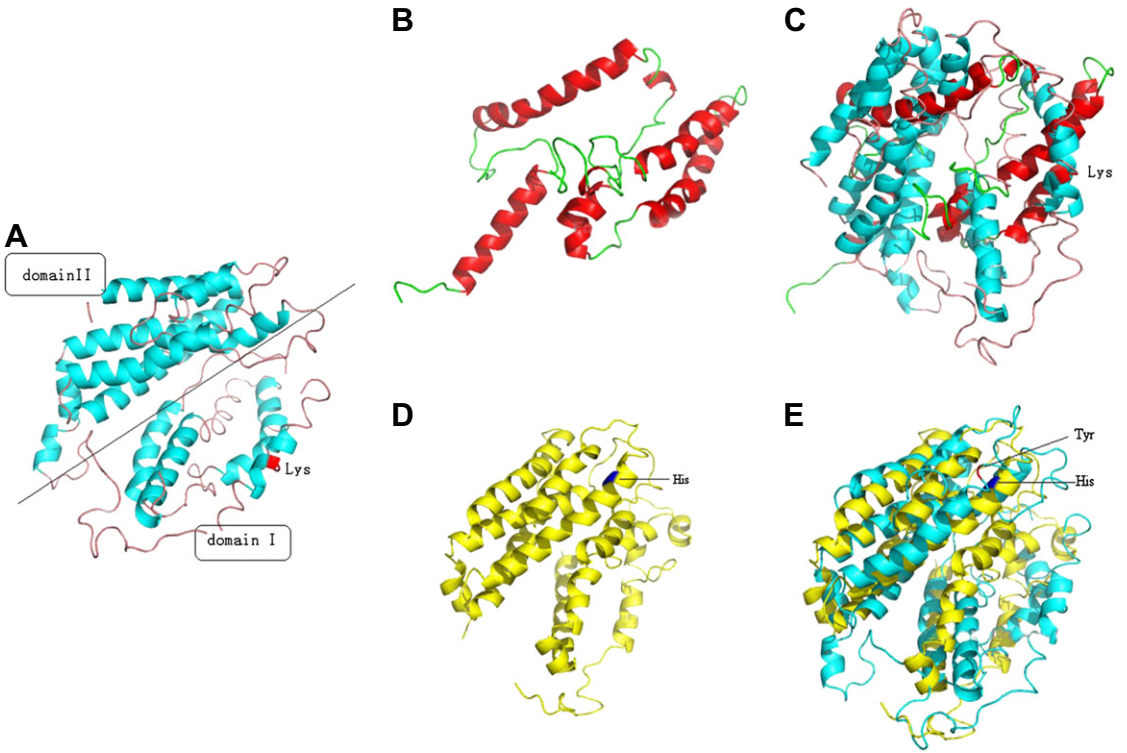

Fig. 4. Predicted 3D structure of wild type SLC34A2 and the two mutants. (A) Wild type SLC34A2, domain II is the transmembrane domain. (B) Truncated mutant caused by the mutation c.910A > T (p.K304X) in exon 8. (C) Overlapping of the truncated protein with the wild type SLC34A2. (D) Mutated protein caused by the mutation c.1363T > C(p. Y455H)in exon 12. (E) Overlapping of the wild type SLC34A2 with the mutant containing the point mutation.

We found that the wild type SLC34A2 protein consists of 690 amino acids, which forms two domains and Domain II is the trans-membrane domain (Fig. 4A). The mutant caused by mutation c.910A > T (p. K304X) in exon 8 leads to protein truncation, and the truncated protein has a length of only 303 amino acids (Fig. 4B). Overlapping of this truncated protein with the wild type showed that these two proteins share very few common functional regions (Fig. 4C). Mutation c.1363T > C (p. Y455H) in exon 12 resulted in a point mutation of TAT (Tyrosine) to CAT (Histidine). Although this mutation did not lead to a length change of the protein (Fig. 4D), it caused an irregular coil formation in the trans-membrane domain, as well as in the domain I (Fig. 4E).

Discussion

In this study, we identified a compound heterozygous mutation of the *SLC34A2* gene in a PAM patient, and computationally predicted 3D structures of the mutants.

Although the etiology of PAM was unclear, the incidence of the familial occurrence of the disease is high, ranging from about 30% to 50% of all the cases reported. PAM often affects horizontal siblings from inbred families, suggesting that this is an autosomal recessive disease (Hagiwara and Tachibana, 2010). Despite the versatile mutation symbols, homozygous mutation is the most common genotype and protein truncation is the predominant form of these mutations. Our patient exhibited a mutation symbol that is completely different from previous reported cases. This compound heterozygous mutation resulted in the expression of two different mutated proteins. The mutation of c.910A > T (p. K304X) in exon 8 leads to a premature termination in the C-terminal region, as been previously reported (Wang et al., 2010; Zhong et al., 2009). The mutation in exon 12 caused a point mutation, which has not been reported before. Further familial analysis revealed that the father carried the mutation of c.910A > T (p. K304X) in exon 8, and the mother carried the mutation of c.1363T > C (p. Y455H) in exon 12. Nevertheless, the clinical manifestation of this patient is similar to other patients with homozygous mutation, indicating that both mutations caused the functional loss of the protein.

The functions of the mutated SLC34A2 proteins are not well known. Among all those previous reports, only Hunqun et al. performed a functional study through an assay of phosphate uptake by Xenopus oocytes, which were engineered to express either wild type or mutated *SLC34A2* genes (Huqun et al., 2007). However, this study did not provide information about functional regions of the wild type or mutated proteins. Furthermore, the technique of in vitro microinjection is time-consuming and costly, limiting its application in such versatile mutation symbols. In the present study, we took the advantage of the bioinformatic technology and predicted 3D structures of the proteins in a quicker and reliable way by using online softwares. In the predicted 3D structure image, the residual segments of the truncated mutant displayed little overlap with the wild type SLC34A2 protein, suggesting a significant functional change of this mutant. While the protein with the point mutation displayed a decent overlap with that of the wild type in the 3D image, the mutation from Tyrosine to Histidine results in a remarkable local structure change of the α helix, possibly because of the appearance of the positive charge at the residue 455. This result suggested that the amino acid (aa455) as well as the relevant domain is likely functionally important for the SLC34A2 protein.

PAM pathogenesis is characterized by an early onset and very slow development. Although full penetrance of genetic defect has been noticed in the development of PAM (Corut et al., 2006), non-genetic environmental factors seem to play an important role in the progression of this disease. Heavy smokers seem to have severer phenotype (Corut et al., 2006). Infection might also accelerate the progression. The symptoms of our patient progressed fast within one year, which might be attributable to his long history of heavy smoking. Although extra-pulmonary calcification has been reported in some patients with PAM (Jonsson et al., 2012; Sosman et al., 1957), the pathology of our patient is limited to the lung.

Another phenomenon worth mentioning is that patients with different races tend to exhibit distinct mutation sites. Mutation sites of patients from Turkey were often on multiple exons; those of Japanese patients were mainly on exons 7 and 8. However, mutation sites of Chinese patients were found on the exon 8 prior to this study. In our previous studies, we analyzed gene mutation sites in Chinese patients with PAM and postulated that exon 8 might be the main target for PAM screening in China. The current study further confirmed that exon 8 is the main mutation site, and in addition, exon 12 may represent another target that needs attention.

In conclusion, we have identified a compound heterozygous mutation of the *SLC34A2* gene in a non-inbred Chinese PAM patient. We also analyzed the functional regions of the wild type and two mutants of the *SLC34A2* gene for the first time through a computational 3D protein structure prediction. Together with our previous work (Yin et al., 2013), this study further suggested that exon 8 might be the main susceptibility loci of Chinese PAM patients. Identification of genetic mutations plus computational prediction of 3D structures of the mutants may represent a novel supporting diagnostic strategy for patients that are highly suspicious of developing PAM. And this strategy may also be used as a means to estimate prognosis for established PAM patients.

Acknowledgments

We thank the family members for their participation in this study and their consent to publishing the data. We also thank Dr. Xiaoyong Lu and Dr. Tao Xia for their help with this study. This study was supported by Zhejiang Provincial Science and Technology Project No. 2011C37073 to H. Wang.

References

Corut, A., Senyigit, A., Ugur, S.A., Altin, S., Ozcelik, U., Calisir, H., et al., 2006. Mutations in SLC34A2 cause pulmonary alveolar microlithiasis and are possibly associated with testicular microlithiasis. Am. J. Hum. Genet. 79, 650–656.

Dogan, O.T., Ozsahin, S.L., Gul, E., Arslan, S., Koksal, B., Berk, S., et al., 2010. A frame-shift mutation in the SLC34A2 gene in three patients with pulmonary alveolar microlithiasis in an inbred family. Intern. Med. 49, 45–49.

Hagiwara, K.J.T., Tachibana, T., 2010. Pulmonary alveolar microlithiasis. Molecular Basis of Pulmonary Disease, Insight from Rare Lung Disorders, pp. 325–338.

Hashimoto, M., Wang, D.Y., Kamo, T., Zhu, Y., Tsujiuchi, T., Konishi, Y., et al., 2000. Isolation and localization of type IIb Na/Pi cotransporter in the developing rat lung. Am. J. Pathol. 157, 21–27.

Huqun, Izumi, S., Miyazawa, H., Ishii, K., Uchiyama, B., Ishida, T., et al., 2007. Mutations in the SLC34A2 gene are associated with pulmonary alveolar microlithiasis. Am. J. Respir. Crit. Care Med. 175, 263–268.

Ishihara, Y., Hagiwara, K., Zen, K., Huqun, Hosokawa, Y., Natsuhara, A., 2009. A case of pulmonary alveolar microlithiasis with an intragenetic deletion in SLC34A2 detected by a genome-wide SNP study. Thorax 64, 365–367.

Jonsson, A.L., Hilberg, O., Bendstrup, E.M., Mogensen, S., Simonsen, U., 2012. SLC34A2 gene mutation may explain comorbidity of pulmonary alveolar microlithiasis and aortic valve sclerosis. Am. J. Respir. Crit. Care Med. 185, 464.

Kelley, L.A., MacCallum, R.M., Sternberg, M.J., 2000. Enhanced genome annotation using structural profiles in the program 3D-PSSM. J. Mol. Biol. 299, 499–520.

Mariotta, S., Ricci, A., Papale, M., De Clementi, F., Sposato, B., Guidi, L., et al., 2004. Pulmonary alveolar microlithiasis: report on 576 cases published in the literature. Sarcoidosis Vasc. Diffuse Lung Dis. 21, 173–181.

Ozbudak, I.H., Bassorgun, C.I., Ozbilim, G., Luleci, G., Sarper, A., Erdogan, A., et al., 2012. Pulmonary alveolar microlithiasis with homozygous c.316G > C (p.G106R) mutation: a case report. Turk Patoloji Derg. 28, 282–285.

Proesmans, M., Boon, M., Verbeken, E., Ozcelik, U., Kiper, N., Van de Casseye, W., et al., 2012. Pulmonary alveolar microlithiasis: a case report and review of the literature. Eur. J. Pediatr. 171, 1069–1072.

Puhr, L., 1933. Mikrolithiasis alveolaris pulmonum. Virchows Arch. Pathol. Anat. Physiol. Klin. Med. 290, 156–160.

Sali, A., Blundell, T.L., 1993. Comparative protein modelling by satisfaction of spatial restraints. J. Mol. Biol. 234, 779–815.

Sosman, M.C., Dodd, G.D., Jones, W.D., Pillmore, G.U., 1957. The familial occurrence of pulmonary alveolar microlithiasis. Am. J. Roentgenol. Radium Ther. Nucl. Med. 77, 947–1012.

Tachibana, T., Hagiwara, K., Johkoh, T., 2009. Pulmonary alveolar microlithiasis: review and management. Curr. Opin. Pulm. Med. 15, 486–490.

Ucan, E.S., Keyf, A.I., Aydilek, R., Yalcin, Z., Sebit, S., Kudu, M., et al., 1993. Pulmonary alveolar microlithiasis: review of Turkish reports. Thorax 48, 171–173.

Vaguine, A.A., Richelle, J., Wodak, S.J., 1999. SFCHECK: a unified set of procedures for evaluating the quality of macromolecular structure-factor data and their agreement with the atomic model. Acta Crystallogr. D Biol. Crystallogr. 55, 191–205.

Wang, H., Yin, X., Wu, D., 2010. Novel human pathological mutations. SLC34A2. Disease: pulmonary alveolar microlithiasis. Hum. Genet. 127, 471.

Yin, X., Wang, H., Wu, D., Zhao, G., Shao, J., Dai, Y., 2013. SLC34A2 gene mutation of pulmonary alveolar microlithiasis: report of four cases and review of literatures. Respir. Med. 107, 217–222.

Zhong, Y.Q., Hu, C.P., Cai, X.D., Nie, H.P., 2009. A novel mutation of the SLC34A2 gene in a Chinese pedigree with pulmonary alveolar microlithiasis. Zhonghua Yi Xue Yi Chuan Xue Za Zhi 26, 365–368.